Polysulfone-*graft*-poly(*tert*-butyl acrylate): Synthesis, Nanophase Separation, Poly(*tert*-butyl acrylate) Hydrolysis, and pH-Dependent Iridescence

Zhihua Lu and Guojun Liu*

Department of Chemistry, University of Calgary, 2500 University Drive, NW, Calgary, Alberta, Canada T2N 1N4

Scott Duncan

Defence Research Development Canada−Suffield, PO Box 4000 Station Main, Medicine Hat, Alberta, Canada T1A 8K6

Received July 12, 2003; Revised Manuscript Received October 24, 2003

ABSTRACT: Polysulfone-*graft*-poly(*tert*-butyl acrylate) or PSf-*g*-P*t*BA samples were prepared by reacting lithiated Udel polysulfone (PSf) in THF at −78 °C with bromine-end-functionalized poly(*tert*-butyl acrylate) or P*t*BA-Br. In bulk, the P*t*BA branches segregated from the PSf backbone to form nanometer-sized domains. The P*t*BA domain shape changed from wormlike to cylindrical and to lamellar as its volume fraction increased from 19.2% to 44%. While the wormlike and cylindrical morphologies lacked long-range order, the alternating P*t*BA and PSf lamellae were packed regularly. The P*t*BA domains in such graft copolymer films could be hydrolyzed to yield poly(acrylic acid) or PAA chains without affecting film integrity. After P*t*BA hydrolysis, a sample with a P*t*BA volume fraction of 38% showed iridescence or a 1-D photonic stop band at ∼450 nm in basic water. The iridescence could be turned off and on by cycling pH between 2 and 10, for example.

I. Introduction

The different components of a block[1] or graft copolymer may segregate in bulk, yielding nanometer-sized patterns or mesophasic structures. There are many applications for the nanodomained solids. Matching the periodicity of the patterns with the wavelength of visible light, Thomas and co-workers have demonstrated that block copolymer solids, before or after chemical processing, functioned as photonic crystals.[2] By using lithographic techniques, a Princeton group has transferred 2-D patterns formed by diblocks to the surfaces of other substrate to yield high-density information storage bits.[3] Segregated block copolymer solids have also been used as precursors for the preparation of various nanostructures including nanospheres,[4,5] nanofibers,[6] nanotubes,[7] and thin films containing nanochannels.[8,9] Thin films containing nanochannels have been used as membranes,[9b] as pH sensors,[8c] or as templates to prepare metallic nanorods.[8c,9c]

Thin films containing regularly packed nanochannels are prepared from diblocks in which one of the components is partially[8] or fully degradable.[9] The diblock composition is so chosen that the degradable block forms cylindrical or gyroidal domains dispersed in the matrix of the other block. Nanochannels are formed by chemically removing the cylindrical or gyroidal domains with or without cross-linking the matrix block. For membrane applications, the nanochannel-containing thin films prepared should be strong and tough. Thus, the matrix block should be made of a high-performance polymer like Udel polysulfone. Many high-performance polymers are prepared by condensation polymerization and contain functionality like esters and ketones. The preparation of block copolymers containing such blocks is technically challenging. The branches and backbone of a graft copolymer may segregate as well. It may be possible to prepare nanochanneled membranes with much more superior mechanical properties starting with graft copolymers. In this paper, we report on the preparation of two polysulfone-*graft*-poly(*tert*-butyl acrylate) or PSf-*g*-P*t*BA samples (Scheme 1) by reacting bromo-end-functionalized P*t*BA or P*t*BA-Br with lithiated Udel polysulfone. We also report on the phase separation properties of these two samples and their mixtures.

We chose P*t*BA as the branched component as it can readily hydrolyze to poly(acrylic acid) or PAA. Membranes containing PAA-lined nanochannels may facilitate water or water vapor transport. The pH-dependent conformation change of the PAA chains may enable gated water flow as has been demonstrated for other types of PAA-containing membranes.[8c,10] In this paper, we report on our preliminary progress in preparing PSf-*g*-P*t*BA and PSf-*g*-PAA membranes and the development of a method for hydrolyzing the P*t*BA domains while retaining the integrity of the PSf-*g*-P*t*BA film. We conclude by reporting our serendipitous discovery that membranes of a PSf-*g*-PAA sample containing alternating PAA and PSf lamellae showed pH-dependent iridescence.

II. Experimental Section

Materials. Polysulfone (Udel P3500) was a generous gift from Solvay Advanced Polymers. Before use, it was dissolved in dichloromethane and precipitated into hexane. This purification procedure was repeated twice, and the final precipitate was dried under vacuum at 120 °C for 12 h. 1,1-Diphenylethylene (DPE) was vacuum-distilled in the presence of butyllithium. 1,2-Dibromoethane was washed with concentrated sulfuric acid for five times and water thrice, dried over magnesium sulfate, and vacuum-distilled. It was distilled from CaH_2 again just before use. Monomer *tert*-butyl acrylate (*t*BA) was distilled under vacuum over CaH_2 and then in the

10.1021/ma034980u CCC: $27.50
Published on Web 12/06/2003

Scheme 1. Structure of PSf-*g*-P*t*BA

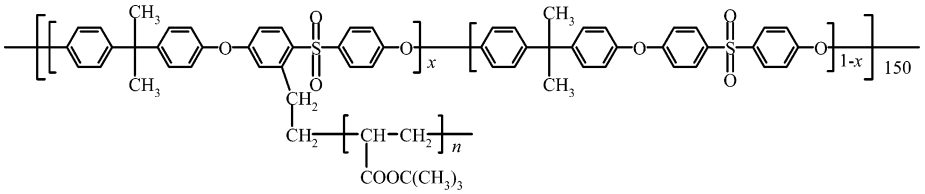

presence of triethylaluminum. Tetrahydrofuran (THF) was dried by refluxing with potassium and a small amount of benzophenone until a deep purple color developed and was distilled just before use. Other chemicals were used as received.

P*t*BA-Br Preparation and Purification. Two P*t*BA-Br samples were prepared by anionic polymerization using an excess of 1,2-dibromoethane as the terminator. The two samples have the weight-average repeat units, n_w, of 340 and 90, respectively, and are denoted as P*t*BA_{340}-Br and P*t*BA_{90}-Br. To prepare P*t*BA_{90}-Br, LiCl (1.45 g, 34.1 mmol) was added into a 1 L round-bottomed flask, and the flask was flamed under vacuum. Following this, dry THF (500 mL) and DPE (0.90 mL, 5.12 mmol) were added into the flask; the solution was immersed in a dry ice/acetone bath at −78 °C. At this stage, *sec*-BuLi, 1.3 M in hexane, was added dropwise until light pink color was observed. Then, another 2.63 mL of the *sec*-BuLi solution (3.42 mmol) was added. After stirring for 15 min, *t*BA (40.0 mL, 297 mmol) was added. The polymerization was allowed to proceed for half an hour before the resultant mixture was pressured through an 18 gauge needle into a mixture containing 10 mL of 1,2-dibromoethane in 100 mL of THF at −40 °C. The mixture was stirred for 2 h and then warmed to room temperature. The solvent was removed by rotaevaporation. The solid residue was redissolved in THF and precipitated into iced water. The precipitated polymer was dried under vacuum at 60 °C for 12 h. P*t*BA_{340}-Br was prepared similarly except that an excess of neat 1,2-dibromoethane was added into the final reaction mixture to terminate *t*BA polymerization. We did not transfer the polymerization mixture by a needle into a terminator solution as the viscosity of the polymerization mixture was too high.

Synthesis of PSf-*g*-P*t*BA. Several PSf-*g*-P*t*BA samples were prepared, and only two of them, PSf-*g*-P*t*BA_{90} and PSf-*g*-P*t*BA_{340} with characteristics to be given later, were used for the morphological studies. An example procedure involved dissolving 6.00 g of PSf (13.6 mmol of Sf units) in 450 mL of dry THF in a 1 L round-bottomed flask. BuLi (0.68 mL, 10.0 M in hexane) was injected over 10 min at −78 °C. After 2 h, 4.00 g of P*t*BA_{90}-Br in 50 mL of dry THF was added. The mixture was stirred at −78 °C for 3 days before 1.0 mL of acetic acid and 1.0 mL of methanol in 2.0 mL of THF were added to annihilate the excess lithiated sites on PSf. After warming to room temperature, the solution was added into iced water to precipitate out the polymer. The polymer was filtered and stirred in methanol for 12 h to extract the unreacted P*t*BA_{90}-Br and then separated from the extract by centrifugation. This process was repeated several times until the methanol phase contained no polymer, which was judged from a turbidity test after adding the methanol phase into water. The extracted solid was dried at 60 °C under vacuum overnight to yield 7.3 g of copolymer. The composition of the polymer was analyzed by NMR.

To obtain the kinetic data for P*t*BA_{90}-Br grafting, samples were taken at different times. The samples were purified following the procedure mentioned above and then analyzed for grafted P*t*BA. PSf-*g*-P*t*BA_{340} was purified by dissolving it in THF and then precipitating it into methanol/water (v/v = 95/5), which solubilized P*t*BA_{340}-Br.

PSf-*g*-P*t*BA Films. PSf-*g*-P*t*BA films were obtained by evaporating the polymer solution in CH_2Cl_2. In an example preparation, 0.150 g of PSf-*g*-P*t*BA_{340} was dissolved in 5.0 mL of dichloromethane. The solution was filtered through a 0.45 μm Teflon filter and poured into a cylindrical ring with a diameter of 6.2 cm glued by poly(vinyl alcohol) on to a leveled glass plate. The solution was covered with another glass plate and allowed to evaporate over 3−7 days. The cover was then removed, and the membrane was further dried for 2 days. After soaking in water the 35 μm thick membrane was peeled off from the glass plate and was dried under vacuum for 6 h again.

Cleavage of the *tert*-Butyl Groups in the PSf-*g*-P*t*BA Films. PSf-*g*-P*t*BA films, 20−50 μm thick, were immersed in a mixture of trifluoroacetic acid and formic acid (v/v = 1/4) for 24 h to cleave the *tert*-butyl group. The membrane was then washed with water and dried under vacuum for 6 h.

Polymer Characterization. The weight-average molar mass M_w of P*t*BA_{90}-Br, P*t*BA_{340}-Br, and PSf was measured by light scattering (LS) using a Brookhaven model 9025 instrument equipped with a 632.8 nm He−Ne laser. THF and methanol were used as solvents for PSF and P*t*BA-Br, respectively. The solutions were clarified by passing through 0.1 μm filter. The difference, Δn_r, between the refractive index of a polymer solution and the solvent was determined using a differential refractometer (Precision Instruments) with light that had passed a band-pass filter centered at 633 nm. Size exclusion chromatography (SEC) analysis was performed on a Waters system equipped with a HT-4 column using THF as the eluant at 30 °C. Molecular weight and polydispersity were calculated on the basis of poly(methyl methacrylate) standards.

Transmission Electron Microscopy. PSf-*g*-P*t*BA or PSf-*g*-PAA films obtained after *tert*-butyl group cleavage were sandwiched by two polystyrene plates (1.5 mm thick) and heated for several minutes at 120 °C to fuse the plates. After cooling, the sandwiched film was microtomed using an Ultracut-E Reichert-Jung instrument to yield thin sections with thickness ∼50 nm, which were picked up by Formvar-coated copper grids. The PSf-*g*-PAA thin sections were stained with a 3.0 wt % uranium acetate $U(Ac)_2$ solution in ethanol/water (v/v = 1/9) for 15 min and rinsed with water thrice before being viewed by a Hitachi-700 electron microscope operated at an accelerated voltage of 75 kV. The PSf-*g*-P*t*BA thin sections were stained with RuO_4 vapor for 4 h.

III. Results and Discussion

Characterization of the Polymer Precursors. Table 1 summarizes the characterization results for P*t*BA_{90}-Br, P*t*BA_{340}-Br, and PSf. The $\Delta n_r/c$ values were plotted as a function of polymer concentration c.[11] Extrapolating the $\Delta n_r/c$ data to zero concentration yielded the refractive index increments dn_r/dc of 0.097 and 0.120 mL/g for P*t*BA_{90}-Br and P*t*BA_{340}-Br in methanol. The dn_r/dc values were then used in combination with light scattering data to yield the weight-average molar masses for the samples. The dn_r/dc and M_w values of PSf were determined in THF.

The absolute polydispersity indices M_w/M_n determined by SEC are not reliable because the calibration standards that were used were PMMA. For the two P*t*BA-Br samples, the M_w/M_nvalues do offer a valid measure of their relative polydispersity. The M_w/M_nvalue of P*t*BA_{340}-Br was larger than that for P*t*BA_{90}-Br. This occurred because the preparation of the former involved adding the terminator 1,2-dibromoethane into the P*t*BA anion solution. Polymerization of the latter was terminated by adding the P*t*BA anion solution into a 1,2-dibromoethane solution. In the former case, more P*t*BA chain dimerization was expected. In the absence of an

Scheme 2. Lithiation of PSf

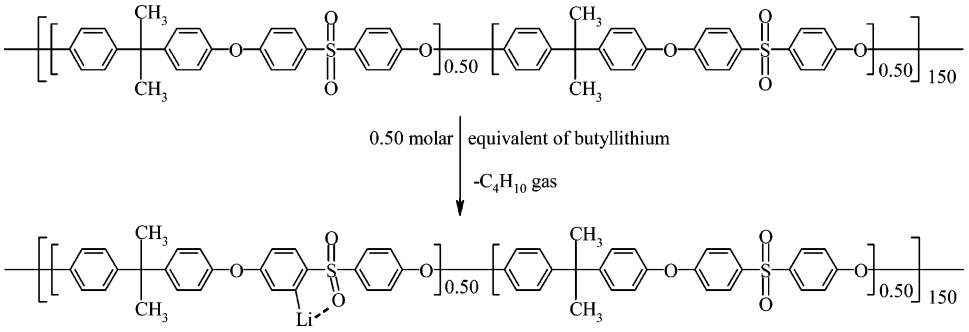

Table 1. Characteristics of P*t*BA and PSf

sample	dn_r/dc (mL/g)	$10^{-4}M_w$ (g/mol)	SEC n_w	SEC M_w/M_n	SEC n_n
P*t*BA$_{90}$-Br	0.097	1.11	90	1.26	71
P*t*BA$_{340}$-Br	0.120	4.3	340	1.40	242
PSf	0.202	6.8	150	1.67	90

absolute technique in our laboratory for determining M_n, we used SEC M_w/M_n to estimate M_n and thus the number-average numbers of repeat units, n_n, for the different samples. The polydispersity M_w/M_n of 1.67 for PSf is in error and much smaller than 3.80 reported by the supplier[12] because we did not include the less than ~5 wt % of cyclic dimer, trimer, and tetramer impurities in the SEC $\boldsymbol{M}_w$ and M_n analysis.

Preparation and Characterization of PSf-*g*-P*t*BA. Three methods are generally used to prepare graft copolymers as reviewed by Pitsikalis et al.[13] These include the grafting "onto" method, grafting "from" method, and macromer method. Both the grafting onto[14] and grafting from[15] methods have been used to prepare PSf-containing graft copolymers. In the grafting from method, functional groups were introduced to the aryl groups of PSf and then used to initiate the polymerization of other monomers. We prepared PSf-*g*-P*t*BA by reacting P*t*BA-Br with lithiated PSf using the graft onto method. Lithiated PSf was prepared by reacting PSf with *n*-butyllithium (BuLi) at a Sf to BuLi molar ratio of 1.00/0.50. Studies reported in the literature[16] show that the lithiation occurred mainly at the ortho position (Scheme 2) relative to the sulfone group because of its strong electron-withdrawing effect and the ability of the lone pairs of electrons on the sulfone oxygen atoms to complex with lithium. Lithiated PSf and the terminal alkyl halide groups of P*t*BA reacted most likely via the S_2N mechanism.

SEC was used to monitor the progress of the reaction. Without purification, a crude sample comprised P*t*BA-Br, PSf-*g*-P*t*BA, and probably PSf. Its size exclusion chromatogram consisted of a sharp P*t*BA-Br peak superimposed on a broad peak of PSf-*g*-P*t*BA and probably PSf. The P*t*BA-Br SEC peak disappeared after sample purification following the procedures described in the Experimental Section.

Table 2 shows the characterization results of the PSf-*g*-P*t*BA$_{90}$ and PSf-*g*-P*t*BA$_{340}$ samples that we prepared in large quantity for morphological studies and also those of two samples named kinetic-2 and kinetic-6 taken from the grafting kinetic run. The fact that the SEC M_w of the grafted samples after the unreacted P*t*BA-Br had been removed were always larger than the M_w value of 100 000 g/mol for PSf shows that the grafting reaction was successful.

Figure 1 shows an NMR spectrum of the kinetic-2 sample and the peak assignments for PSf and P*t*BA. PSf and P*t*BA have distinct peaks, which allowed the easy determination of mass ratio m_{tBA}/m_{Sf} in the grafted samples. The m_{tBA}/m_{Sf} values were then used in combination with the n_n values in Table 1 to yield the number of P*t*BA branches per PSf chain, n_b. Table 2 lists the n_b values calculated for the different samples. The two samples used for morphological studies have a similar n_b value of ~0.85.

Figure 2 shows data from the kinetic run we performed on the grafting reaction between P*t*BA$_{90}$-Br and lithiated PSf. Both n_b and the P*t*BA weight fraction increased in the PSf-*g*-P*t*BA$_{90}$ sample with reaction time t. At reaction equilibrium or at long times, n_b approached ~1.3, which is the same as 1 after possible errors in the M_n values are taken into consideration. The kinetic data suggest that one P*t*BA chain was grafted, on average, onto one PSf chain at −78 °C, despite the much higher P*t*BA-Br/PSf feed ratio used (Table 2). It is possible to increase n_b by increasing the reaction temperature. We did not attempt this as the polymers cross-linked at temperatures higher than around −30 °C.

Nanophase Separation. The different blocks of a diblock copolymer phase segregate if the blocks are sufficiently long so that $N\chi > 10.5$ is satisfied,[1] where N is the total number of monomer units in the diblock and χ is the Flory−Huggins polymer−polymer interaction parameter. The branches and the backbone of a graft copolymer phase segregate also if the branches and backbone chain length between branches are sufficiently long. For an B-*g*-A sample with a large number of A branches, e.g., larger than 8 per B chain, the criterion for phase separation is $(N_A + N_B/n_b)\chi > 10.5$.[17] Here N_A is the number of units in each A branch, N_B is the number of units in the B backbone chain, and N_B/n_b is the number of B chain units between branches. As n_b is reduced to 1, the graft copolymer may become a simple graft copolymer of the form AB_2 where the A chain is grafted to the middle of an B chain. According to Olvera de la Cruz and Sanchez[18] or Milner,[19] the criterion for phase separation in this case is $(N_A + N_B/n_b)\chi > 13.5$. Figure 3 shows the thin-section TEM images of some of the PSf-*g*-P*t*BA samples as a function of P*t*BA volume fraction. The fact that phase separation was observed in every case suggests that $(N_A + N_B/n_b)\chi$ is large for our system.

The densities of P*t*BA and PSf are 1.02[8c] and 1.24 g/mL,[20] respectively. Using these values and the m_{tBA}/m_{Sf} values in Table 2, we calculated the P*t*BA volume fractions of 19.2% and 44% for PSf-*g*-P*t*BA$_{90}$ and PSf-*g*-P*t*BA$_{340}$. To check the P*t*BA morphology variation as a function of volume fraction, we prepared samples with

Table 2. Preparation Conditions and Characteristics of Some PSf-*g*-P*t*BA Samples[a]

sample	m_{tBA}/m_{Sf} in feed	reaction time (h)	m_{tBA}/m_{Sf} (P*t*BA wt %) in copolymer	n_b	SEC M_w (g/mol)	SEC M_w/M_n
P*t*BA$_{90}$-*g*-PSf	7.45/10.0	36	0.20 (16)	0.88	124 000	1.96
P*t*BA$_{340}$-*g*-PSf	13.3/10.0	96	0.65 (39)	0.83	209 000	2.49
		P*t*BA$_{90}$-*g*-PSf samples from the kinetic run				
kinetic-2	4.00/6.00	48	0.25 (20)	1.09	148 000	2.39
kinetic-6	4.00/6.00	168	0.29 (22)	1.27	169 000	2.22

[a] The PSf concentration in THF during the grafting reaction was always 0.0120 g/mL.

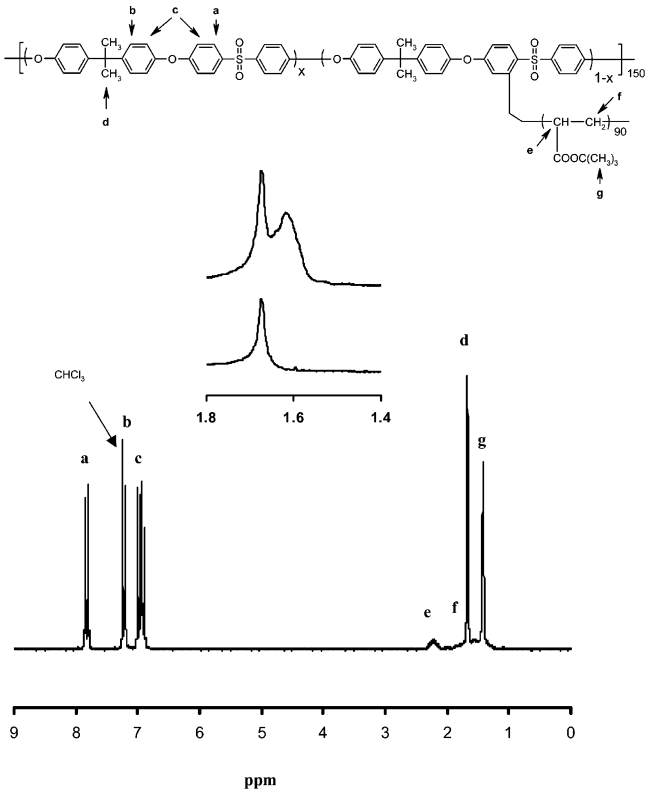

Figure 1. Proton NMR spectrum of the kinetic-2 sample in deuterated chloroform. The inset shows the NMR spectra of the kinetic-2 sample in deuterated pyridine in the 1.4−1.8 ppm region before (top) and after (bottom) *tert*-butyl group removal.

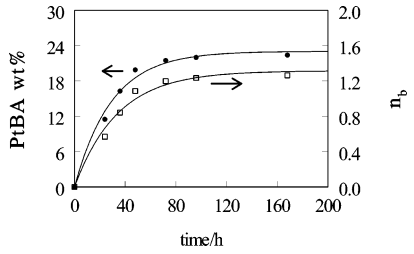

Figure 2. Increase in the P*t*BA weight fraction in a PtBA$_{90}$-*g*-PSf sample or the number of P*t*BA branches per PSf chain as a function of reaction time between PtBA$_{90}$-Br and lithiated PSf. The PSf concentration in THF was 12.0 mg/mL, and the mass ratio between P*t*BA$_{90}$−Br and PSf was 0.400/0.600.

P*t*BA volume fractions between 19.2% and 44% by mixing PSf-*g*-P*t*BA$_{90}$ and PSf-*g*-P*t*BA$_{340}$. Table 3 shows the recipes used for preparing the different mixtures and their characteristics.

Two methods were employed to bring out the contrast between the PSf and P*t*BA domains in our TEM study. In method 1, thin sections of PSf-*g*-P*t*BA were exposed to RuO_4 vapor to stain the PSf domains selectively. Method 2 was more indirect. It involved soaking the films in a mixture of trifluoroacetic and formic acid first

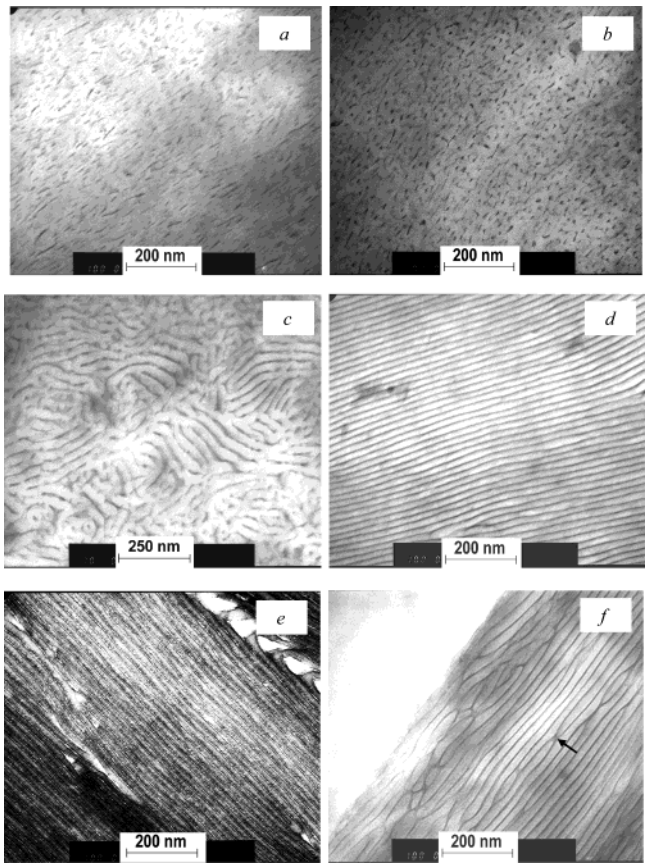

Figure 3. Thin-section TEM images of PSf-*g*-P*t*BA at the P*t*BA volume fractions of 19.2% (a), 23% (b), 30% (c), 38% (d and e), and 44% (f). All images except image e were obtained after staining the samples by method 2. Image e was obtained by staining the sample with method 1.

Table 3. Characteristics of PSf-*g*-P*t*BA Solid Samples

sample	PSf-*g*-P*t*BA$_{90}$ to PSf-*g*-P*t*BA$_{340}$ mass ratio	P*t*BA (wt %)	P*t*BA (vol %)
1	100/0	16.4	19.2
2	85.5/14.5	19.7	23
3	57.8/42.2	26.1	30
4	25.2/74.8	33.5	38
5	0/100	39.3	44

to hydrolyze the P*t*BA domains and then staining the PAA groups with $U(Ac)_2$. We expected the hydrolyzed samples to retain the morphologies of their precursors because PSf is insoluble in the trifluoroacetic and formic acid mixture and the glass transition temperature of PSf is high at 165 °C.[21] The validity of this hypothesis is demonstrated by comparing images d and e in Figure 3 obtained for sample 4 of Table 3 with 38 vol % P*t*BA. Regardless of the staining method used, the same alternating lamellar morphology was observed. The lighter PSf stripes in image d changed into darker stripes in image e, as expected, after the staining agent was switched from the PAA-staining $U(Ac)_2$ to the PSf-

staining RuO_4. Furthermore, the periodicity is comparable at 18.8 and 17.8 nm in images d and e, respectively. We used method 2 mainly for sample staining, because it yielded higher-quality images.

Figure 3 reveals that the P*t*BA morphology changed with its volume fraction. At the volume fractions of 19.2% and 23%, P*t*BA formed a short wormlike phase in the PSf matrix. The P*t*BA morphology changed to cylinders as the volume fraction increased to 30%. Increasing the volume fraction of P*t*BA further to 38% or 44% led to the formation of lamella. While the general trend of P*t*BA morphological change with its volume fraction is similar to that expected for diblocks, the PSf-*g*-P*t*BA morphologies distinctly lacked long-range order, with the exception of the lamellar morphology. This is similar to the trend observed by Gido and Wang[21] for some of their AB_2 simple graft copolymers. Notably, the spherical morphology was not as readily formed at the P*t*BA volume fraction of 19.2% possibly due to the graft copolymer phase diagram shift relative to diblocks, a phenomenon that has also been observed[22] and explained[19] for mikto-arm copolymers of the type A_nB_m and rationalized[17] theoretically for graft copolymers.

We do not intend to rationalize the morphological behavior of the PSf-*g*-P*t*BA samples further because the project is application-oriented and the nonideal constitution of our samples does not warrant a more thorough theoretical analysis. Our samples, which possess nominally 1 branch per chain and consist of a mixture of graft copolymer and PSf, are far from ideal to be the simple graft copolymer AB_2. Our samples are also different from the model adapted by Balaz and co-workers[17] for graft copolymers, as the number of P*t*BA branches changed from PSf chain to chain. Then, the PSf backbone had a wide molar mass distribution. Last, we did not perform any experiments to confirm that the morphologies we observed were the equilibrium ones.

P*t*BA Hydrolysis. P*t*BA hydrolysis in solution should be easy. The challenge was the hydrolysis of the P*t*BA domains in the solid state without affecting the integrity and morphology of the precursory PSf-*g*-P*t*BA films. Our success in doing this was demonstrated by comparing images d and e in Figure 3. To quantify the degree of P*t*BA hydrolysis under the stated conditions, we dissolved the PSf-*g*-PAA films and obtained the NMR spectra for the two samples with the P*t*BA volume fractions of 23% and 38%. In both cases, we found quantitative P*t*BA hydrolysis. This is, for example, shown in the inset of Figure 1, which compares the NMR spectra of the kinetic-2 sample before and after P*t*BA hydrolysis in the 1.4−1.8 ppm region. After P*t*BA hydrolysis in the solid state, the *tert*-butyl peak disappeared completely.

P*t*BA hydrolysis was fast even for the sample with 23 vol % P*t*BA because the PSf matrix swelled in the hydrolyzing mixture consisting of trifluoroacetic and formic acid. We found that the thickness of a PSf membrane swelled from 27 to 30 μm after 4 h soaking in the hydrolyzing mixture.

pH-Dependent PAA Lamellar Expansion and Iridescence. We demonstrated in the previous two subsections the feasibility to tune the morphology of the P*t*BA phase and to hydrolyze this phase without affecting the integrity and morphology of the graft copolymer films. These results suggest the tremendous potential of PSf-*g*-P*t*BA as membrane material. In this subsection, we report and justify our serendipitous discovery that PSf-*g*-PAA membranes derived from films of PSf-*g*-P*t*BA sample 4 with 38 vol % P*t*BA (Table 3) possessed pH-dependent iridescence.

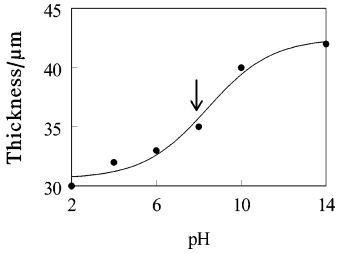

Figure 4. Thickness increase of a PSf-*g*-PAA film with a dry thickness 24 μm derived from PSf-*g*-P*t*BA sample 4 as a function of pH. The arrow indicates the pH after which the iridescence can be seen easily by the naked eye.

The discovery started with our observation that the PSf-*g*-PAA membranes derived from PSf-*g*-P*t*BA samples 4 and 5 swelled substantially in water. We, for example, determined that a 24 μm PSf-*g*-PAA dry film derived from PSf-*g*-P*t*BA sample 4 swelled in pH = 2 water to a thickness of 30 μm. Increasing the pH of the aqueous solution caused further increases in film thickness (Figure 4). We did not obtain the film swelling data for PSf-*g*-PAA films derived from PSf-*g*-P*t*BA sample 5 because the films partially exfoliated in basic water.

The PSf-*g*-PAA film increased in thickness in acidic water most probably due to water uptake by the PAA layers. The film thickness increased further as pH increased because of the increased degree of ionization of the carboxyl groups of PAA. The ionized PAA groups repelled one another and thus pushed the PSf layers farther apart. The different PSf layers did not exfoliate in the case of sample 4 because the PAA content was relatively low. Furthermore, the lamellar structure lacked perfection and the fusion of different PSf lamellae at defective spots, as marked by an arrow in image 3f, aided in preventing PSf layer from exfoliation. This pH-dependent PAA chain conformation change not only gave rise to pH-tunable iridescence but should also be useful in the preparation of membranes with pH-gated flow properties or of drug-loaded membranes with pH-tunable drug release rate.

Iridescence refers to light reflection from a film stack with periodically modulating refractive indices.[23] Iridescence renders metallic luster to a plastic film stack when viewed from certain angles and occurs because of the constructive interference of light reflected from the different layer/layer interfaces in the stack. We noticed iridescence of PSf-*g*-PAA films derived from PSf-*g*-P*t*BA sample 4 above pH ∼8. The left image in Figure 5 shows iridescence from such a film with a dry thickness of 40 μm in pH = 10 water. At the picture-taking angle (∼10° from the film normal direction), only certain regions of the film were iridescent. The right image of Figure 5, which shows that the iridescence substantially dimmed, was taken at a similar angle several minutes after hydrochloric acid was added to the solution to reduce the pH to 2.0. The iridescence at this pH was in fact so weak that it was barely noticeable with the naked eye regardless of the observation angle. More experiments demonstrated that the iridescence could be turned back on once the pH was increased again. This could be cycled many times without noticeable sample performance deterioration. Furthermore, we noticed that the iridescence disappeared even at high pH after a film was pressed mechanically to decrease film swelling. These

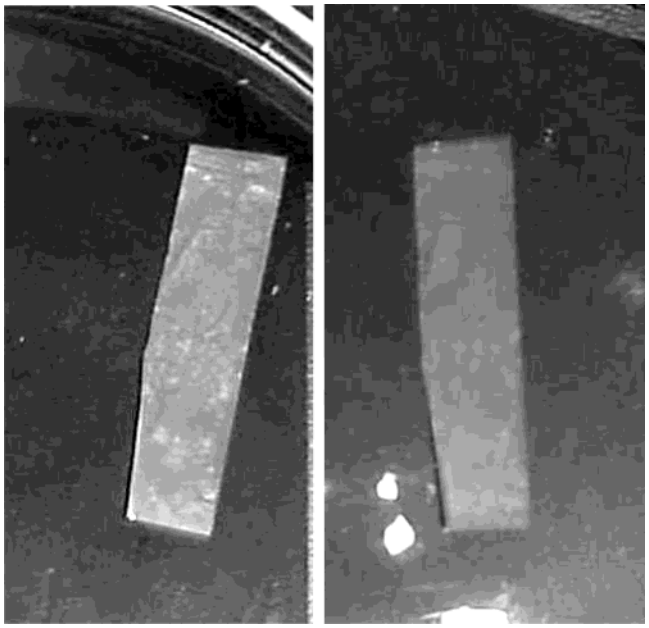

Figure 5. Photographs of a PSf-*g*-PAA film derived from PSf-*g*-P*t*BA sample 4 in pH = 10 (left) and pH = 2 water in a Petri dish.

results suggest the profound potential for using such films as pH or pressure sensors.[24] It is very unfortunate that we presently do not have access to a diffuse reflectance spectrometer to perform a more detailed study of the iridescence properties of the films. We could not have studied the films by a standard UV−vis spectrometer in the transmission mode as we have not prepared uniformly iridescent films yet. It was only by visual comparison of the reflected light with a color chart that we concluded that the wavelength of the reflected light was ∼450 nm.

For a film stack consisting of alternating layers 1 and 2 with refractive indices n_1 and n_2 and thickness d_1 and d_2, iridescence occurs at wavelength λ when the Bragg diffraction equation modified for light applies:

$$\lambda = 2(n_1 d_1 + n_2 d_2) \sin \theta \qquad (1)$$

where θ is the angle formed between the incident light and the film plane. The reflection band of such a film stack is referred to these days as a photonic stop band, and the stack is called a 1-D photonic crystal.[25,26] For light impinging along the normal direction, θ is 90°.

The fact that iridescence occurs at ∼450 nm for our samples suggests that $(n_1 d_1 + n_2 d_2)$ has to be larger than or equal to ∼225 nm. In water at high pH, the PAA chains are ionized and the PAA domains are swollen. The average refractive index n_2 for this layer should be between 1.33 and 1.527 for water and PAA, respectively.[20] The PSf layer should not be significantly swollen and the refractive index n_1 should be close to 1.633 for PSf.[20] From the period of 17.8 nm found from TEM image e in Figure 3 and the volume fraction of 62% for PSf, we estimated a PSf layer thickness d_1 of 11 nm. Using the lower-bound value of 1.333 for the water-swollen PAA layer, the thickness of this layer should be at least 155 nm, according to eq 1, for iridescence to occur. This gives a thickness increase of ∼23 times for the PAA layer in high-pH water. As mentioned before, we observed only a 2-fold thickness increase for the bulk films after soaking them in basic water. This drastic difference between 23 and 2 suggests the nonuniform expansion of the PAA layers from region to region. The nonuniform expansion occurred because only certain lamellar grain orientation or orientations facilitated water and chemical transport. The nonuniform expansion explains also the patchy pattern of the observed iridescence.

We have also noticed that a 40 μm thick dry film had a stronger iridescence than a 20 μm thick dry film in basic water. The efficiency of light reflection or reflectance from a stack of macroscopically aligned parallel layers of equal optical length $n_i d_i$, where $i = 1$ or 2, is given by[27]

$$R = \left[\frac{1 - (n_2/n_1)^N}{1 + (n_2/n_1)^N}\right]^2 \qquad (2)$$

where N is the total number of 1 and 2 bilayers and $n_2 < n_1$. While this equation explains an increase in iridescence intensity with film stack thickness, it is not applicable to our system where $n_1 d_1 \neq n_2 d_2$. Then, the number N may not be determined by thickness of the PSf-*g*-P*t*BA films, as the lamellar grains may not be aligned parallel to the substrate plane.

IV. Conclusions

Different PSf-*g*-P*t*BA samples have been prepared by reacting lithiated PSf with P*t*BA-Br. The weight fraction of P*t*BA in the graft copolymer can be controlled by changing either the number of P*t*BA branches n_b per PSf chain or the length of the P*t*BA-Br chain. The n_b value in a certain range can be changed by varying either the reaction time for a given lithiated PSf and P*t*BA-Br mixture or the mass feed ratio of the two at a given reaction time. The morphology of the P*t*BA branches changes from wormlike to cylindrical and then to lamellar as its volume fraction increases from 19.2% to 44%. While the wormlike and the cylindrical morphologies lack long-range order, the alternating P*t*BA and PSf lamellae are packed regularly. The P*t*BA domains in the PSf-*g*-P*t*BA films are hydrolyzed using a formic and trifluoroacetic acid mixture without affecting the morphology and integrity of the PSf-*g*-P*t*BA precursory films. The PSf-*g*-PAA films derived from PSf-*g*-P*t*BA with 38 vol % P*t*BA show iridescence in basic water. The iridescence intensity can be dimmed by decreasing the solution pH and be turned back on by increasing pH again. This process can be cycled many times without appreciable sample performance deterioration. Alternatively, one can dim the iridescence at high pH by pressing the film mechanically. These results suggest the tremendous potential for using these films in pH and pressure sensing.

Acknowledgment. Defence Research Development Canada is gratefully acknowledged for sponsoring this research.

References and Notes

(1) See, for example: Bates, F. S.; Fredrickson, G. H. *Phys. Today* **1999**, February, 32.
(2) (a) Urbas, A. M.; Maldovan, M.; DeRege, P.; Thomas, E. L. *Adv. Mater.* **2002**, *14*, 1850. (b) Edrington, A. C.; Urbas, A. M.; DeRege, P.; Chen, C. X.; Swager, T. M.; Hadjichristidis, N.; Xenidou, M.; Fetters, L. J.; Joannopoulos, J. D.; Fink, Y.; Thomas, E. L. *Adv. Mater.* **2001**, *13*, 1853.
(3) Park, M.; Harrison, C.; Chaikin, P. M.; Register, R. A.; Adamson, D. H. *Science* **1997**, *276*, 1401.

(4) Saito, R.; Fujita, A.; Ichimuru, A.; Ishizu, K. *J. Polym. Sci., Part A: Polym. Chem.* **2000**, *38*, 2091.
(5) Erhardt, R.; Boker, A.; Zettl, H.; Kaya, H.; Pyckhout-Hintzen, W.; Krausch, G.; Abetz, V.; Muller, A. H. E. *Macromolecules* **2001**, *34*, 1069.
(6) See, for example: (a) Liu, G. J.; Qiao, L. J.; Guo, A. *Macromolecules* **1996**, *29*, 5508. (b) Liu, G. J.; Ding, J. F.; Qiao, L. J.; Guo, A.; Gleeson, J. T.; Dymov, B.; Hashimoto, T.; Saijo, K. *Chem.—Eur. J.* **1999**, *5*, 2740. (c) Massey, J.; Power, K. N.; Manners, I.; Winnik, M. A. *J. Am. Chem. Soc.* **1998**, *120*, 9533. (d) Won, Y.-Y.; Davis, H. T.; Bates, F. S. *Science* **1999**, *283*, 960. (e) Templin, M.; Franck, A.; DuChesne, A.; Leist, H.; Zhang, Y. M.; Ulrich, R.; Schadler, V.; Wiesner, U. *Science* **1997**, *278*, 5344.
(7) (a) Stewart, S.; Liu, G. J. *Angew. Chem., Int. Ed.* **2000**, *39*, 340. (b) Yan, X. H.; Liu, F. T.; Li, Z.; Liu, G. J. *Macromolecules* **2001**, *34*, 9112.
(8) (a) Liu, G. J.; Ding, J. F.; Guo, A.; Herfort, M.; Bazett-Jones, D. *Macromolecules* **1997**, *30*, 1851. (b) Liu, G. J.; Ding, J. F. *Adv. Mater.* **1998**, *10*, 69. (c) Liu, G. J.; Ding, J. F.; Hashimoto, T.; Saijo, K.; Winnik, F. M.; Nigam, S. *Chem. Mater.* **1999**, *11*, 2233. (d) Liu, G. J.; Ding, J. F.; Stewart, S. *Angew. Chem., Int. Ed.* **1999**, *38*, 835.
(9) (a) Lee, J.-S.; Hirao, A.; Nakahama, S. *Macromolecules* **1989**, *22*, 2602. (b) Zalusky, A. S.; Olayo-Valles, R.; Taylor, C. J.; Hillmyer, M. A. *J. Am. Chem. Soc.* **2001**, *123*, 1519. (c) Thurn-Albrecht, T.; Schotter, J.; Kastle, G. A.; Emley, N.; Shibauchi, T.; Krusin,-Elbaum, L.; Guarini, K.; Black, C. T.; Tuominen, M. T.; Russell, T. P. *Science* **2000**, *290*, 2126. (d) Hashimoto, T.; Tsutsumi, K.; Funaki, Y. *Langmuir* **1997**, *13*, 6869.
(10) (a) Hautojarvi, J.; Kontturi, K.; Nasman, J. H.; Svarfvar, B. L.; Viinikka, P.; Vuoristo, M. *Ind. Eng. Chem. Res.* **1996**, *35*, 450. (b) Winnik, F. M.; Morneau, A.; Mika, A. M.; Childs, R. F.; Roig, A.; Molins, E.; Ziolo, R. F. *Can. J. Chem.* **1998**, *76*, 10.
(11) Huglin, M. B. *Light Scattering from Polymer Solutions*; Academic Press: London, 1972.
(12) Savariar, S.; Underwood, G. S.; Dicknson, E. M.; Schielke, P. J.; Hay, A. S. *Desalination* **2002**, *144*, 15.
(13) Pitsikalis, M.; Pispas, S.; Mays, J. W.; Hadjichristidis, N. *Adv. Polym. Sci.* **1998**, *135*, 1.
(14) Nagase, Y.; Naruse, A.; Matsui, K. *Polymer* **1989**, *60*, 1931.
(15) (a) Lee, W. H.; Lee, S. *J. Macromol. Sci. Chem.* **1988**, *A25*, 705. (b) Xiao, G. Y.; Zhu, S. M.; Yan, D. Y.; Xu, J. L. *Polym. Int.* **2002**, *51*, 673.
(16) Guiver, M. D.; Robertson, G. P.; Yoshikawa, M.; Tam, C. M. In *Membrane Formation and Modification*; ACS Symposium Series 744; Pinau, I., Freeman, B. D., Eds.; American Chemical Society: Washington, DC, 2000.
(17) (a) Shinozaki, A.; Jasnow, D.; Balazs, A. C. *Macromolecules* **1994**, *27*, 2496. (b) Foster, D. P.; Jasnow, D.; Balazs, A. C. *Macromolecules* **1995**, *28*, 3450.
(18) Olverra de la Cruz, M.; Sanchez, I. C. *Macromolecules* **1986**, *19*, 2501.
(19) Milner, S. T. *Macromolecules* **1994**, *27*, 2333.
(20) Brandrup, J.; Immergut, E. H. *Polymer Handbook*, 3rd ed.; Wiley & Sons: New York, 1989.
(21) Gido, S. P.; Wang, Z. G. *Macromolecules* **1997**, *30*, 6771.
(22) See, for example: Yang, L. Z.; Hong, S.; Gido, S. P.; Velis, G.; Hadjichristidis, N. *Macromolecules* **2001**, *34*, 9069.
(23) See, for example: (a) Alfrey, T., Jr.; Gurnee, E. F.; Schrenk, W. J. *Polym. Eng. Sci.* **1969**, *9*, 400. (b) Jonza, J. M. In *Optical Security and Counterfeit Deterrence Techniques III*; van Renesse, R. L., Vliegenthart, W. A., Eds.; *Proc. SPIE* **2000**, *3973*.
(24) Arsenault, A. C.; Miguez, H.; Kitaev, V.; Ozin, G. A.; Manners, I. *Adv. Mater.* **2003**, *15*, 503.
(25) See, for example: (a) Joannopoulos, J. D.; Villeneuve, P. R.; Fan, S. H. *Nature (London)* **1997**, *386*, 143. (b) John, S. *Phys. Today* **1991**, May, 32.
(26) Urbas, A.; Sharp, R.; Fink, Y.; Thomas, E. L.; Xenidou, M.; Fetters, L. J. *Adv. Mater.* **2000**, *12*, 812.
(27) Born, M.; Wolf, E. *Principles of Optics: Electromagnetic Theory of Propagation, Interference and Diffraction of Light*, 5th ed.; Pergamon Press: Oxford, 1975; p 69.

MA034980U